DOI: 10.1021/ic100623y

Inorganic Chemistry
Article

Trends in Aqueous Hydration Across the 4f Period Assessed by Reliable Computational Methods

Jadwiga Kuta and Aurora E. Clark*

Department of Chemistry, Washington State University, Pullman, Washington 99164

Received April 1, 2010

The geometric and electronic structures, as well as the thermodynamic properties of trivalent lanthanide hydrates $\{Ln(H_2O)_{8,9}^{3+}$ and $Ln(H_2O)_{8,9}(H_2O)_{12,14}^{3+}$, Ln = La−Lu$\}$ have been examined using unrestricted density functional theory (UDFT), unrestricted Möller-Plesset perturbation theory (UMP2), and multiconfigurational self-consistent field methods (MCSCF). While Ln-hydrates with 2−5 unpaired f-electrons have some multiconfigurational character, the correlation energy lies within 5−7 kcal/mol across the period and for varying coordination numbers. As such DFT yields structural parameters and thermodynamic data quite close to experimental values. Both UDFT and UMP2 predict free energies of water addition to the $Ln(H_2O)_8^{3+}$ species to become less favorable across the period; however, it is a non-linear function of the surface charge density of the ion. UDFT further predicts that the symmetry of the metal-water bond lengths is sensitive to the specific f-electron configuration, presumably because of repulsive interactions between filled f-orbitals and water lone-pairs. Within the $Ln(H_2O)_{8,9}(H_2O)_{12,14}^{3+}$ clusters, interactions between solvation shells overrides this orbital effect, increasing the accuracy of the geometric parameters and calculated vibrational frequencies. Calculated atomic charges indicate that the water ligands each donate 0.1 to 0.2 electrons to the Ln(III) metals, with increasing electron donation across the period. Significant polarization and charge transfer between solvation shells is also observed. The relationship between empirical effective charges and calculated atomic charges is discussed with suggestions for reconciling the trends across the period.

Introduction

For the last 50 years, the trivalent lanthanides have been a continued source of interest and inspiration to chemists within the fields of materials science (for magneto-optical solids, ceramics, etc.), nuclear energy (as fission products from the fuel cycle), medicinal chemistry (as MRI contrast agents), and environmental chemistry (in pollutant tracers).[1−6] Within these disciplines, select Ln(III) have their own advantages and have been the focus of much study. For example, the chemistry of Gd^{3+} complexes is well-known as a result of their use as contrast agents.[1−5,7] The solution behavior of Dy^{3+}, Tm^{3+}, and Eu^{3+} complexes have also been thoroughly studied owing to their implementation as shift reagents that separate NMR signals of species in inner- and outer-cellular compartments.[1] However, few studies have specifically examined trends in geometric and electronic properties, or even reactivity across the entire period. Only recently has a homologous series of Ln(III) complexes been synthesized for all 4f elements (except for Pm), revealing that the well-known lanthanide contraction of the ionic radius is best fit by a quadratic function of the number of f-electrons.[8,9] Other empirical studies have looked to varying sets of experimental data to ascertain relationships regarding structure and thermodynamics.[10,11] While it is generally assumed that much similarity exists between the trivalent lanthanides, discrepancies in experimental and theoretical data motivate a thorough investigation regarding trends in electronic structure, geometry, and thermodynamic properties across the entire period. For example, in aqueous solution the experimental metal-water bond lengths early in the period deviate from that predicted by a purely ionic model of the metal-water interaction. The surface charge density, σ, is also used as a guiding parameter in ligand design for extractants of Ln(III)

*To whom correspondence should be addressed. E-mail: auclark@wsu.edu.

(1) Aime, S.; Botta, M.; Fasano, M.; Terreno, E. *Chem. Soc. Rev.* **1998**, *27*, 19.
(2) *Lanthanide probes in life, chemical and earth sciences. Theory and practice*; Bünzli, J.-C. G., Choppin, G. R., Eds.; Elsevier Science Publishers: Amsterdam, The Netherlands, 1989; and refs therein.
(3) Caravan, P.; Ellison, J. J.; McMurry, T. J.; Lauffer, R. B. *Chem. Rev.* **1999**, *99*, 2293.
(4) Lauffer, R. B. *Chem. Rev.* **1987**, *87*, 901.
(5) Peters, J. A.; Huskens, J.; Raber, D. J. *Prog. Nucl. Magn. Reson. Spectrosc.* **1996**, *28*, 283.
(6) *Separations for the nuclear fuel cycle in the 21st century*; Lumetta, G. J., Nash, K. L., Clark, S. B., Friese, J. I., Eds.; ACS Symposium Series; American Chemical Society: Washington, DC, 2006; Vol. *933*.
(7) Brasch, R. C. *Radiology* **1992**, *183*, 1.
(8) Seitz, M.; Oliver, A. G.; Raymond, K. N. *J. Am. Chem. Soc.* **2007**, *129*, 11153.
(9) Yamauchi, S.; Kanno, H.; Akama, Y. *Chem. Phys. Lett.* **1988**, *151*, 315.
(10) David, F. H.; Vokhmin, V. *J. Phys. Chem. A* **2001**, *105*, 9704.
(11) David, F. H. *Radiochim. Acta* **2008**, *96*, 135.

Published on Web 08/02/2010

from other fission products of the nuclear fuel cycle. Yet the trends in σ across the period are a topic of some dispute. Finally, a fundamental understanding of the lanthanides is highly beneficial from a kinetic perspective, since the exchange rates of waters in the primary solvation shell with those in the secondary shell are an upper bound to ligand complexation rates. In this work, gas-phase and solution continuum calculations have examined all Ln(III) with first and second solvation shells. Select structural and thermodynamic properties have been benchmarked against experimental data, while a combination of multiconfigurational wave function, perturbation, and density functional theory methods have investigated trends in hydrogen-bonding networks, atomic charge and surface charge density, bonding interactions with hydrating water ligands, and other characteristics of solvation across the 4f period. Our most important conclusions illustrate a complexity within the electronic, thermodynamic, and structural properties of aqueous Ln(III) that has previously been omitted within the literature.

Computational Methods

All calculations were performed with the NWChem[12] and Gaussian 03[13] packages. On the basis of our prior work,[14−16] we have found that the B3LYP[17] and TPSS[18] functionals yield very good geometric and thermodynamic properties for trivalent La, Ce, and Lu. As such these functionals have been employed for the optimization of $Ln(H_2O)_{8,9}^{3+}$ and select $Ln(H_2O)_{8,9}(H_2O)_{12,14}^{3+}$ complexes. The size of the second solvation shell is based upon initial optimizations of $Ln(H_2O)_8(H_2O)_{16}^{3+}$ and $Ln(H_2O)_9(H_2O)_{18}^{3+}$ wherein it was observed that four waters migrated into a third solvation shell. The optimized geometries of the $(H_2O)_{8,9}$ and $(H_2O)_{21,22}$ clusters were taken from our prior work.[14] The Stuttgart RSC28 relativistically corrected effective core potential (RECP) was employed for Ln(III) which replaces the 28 inner-shell electrons with a pseudopotential.[19,20] The corresponding Stuttgart basis on the Ln(III) consisted of a segmented contracted 9s8p5d4f3g basis. The aug-cc-pVDZ basis set was employed for all H and O.[21] Geometry optimizations in NWChem employed an SCF energy convergence criterion of 10^{-6}, an integral internal screening threshold of 10^{-16}, a numerical integration grid of 10^{-8}, and a tolerance in Schwarz screening for the Coulomb integrals of 10^{-12}. Following geometry optimization, frequency calculations were performed to obtain thermochemical corrections as well as to ensure that all structures correspond to local minima; no imaginary vibrations or a single imaginary vibrational mode less than 20 cm^{-1} were found. Geometry optimization and/or frequency calculation files for all of the hydrated species may be found on the Computational Actinide and Nuclear Science database housed at Washington State University: http://cans.wsu.edu. To analyze the electronic structure resulting from the UDFT calculations, a modified natural population analysis (NPA) was performed,[15] which has the 6s6p5d4f natural atomic orbitals (NAOs) within the valence space. The complete active space self-consistent field (CASSCF) method,[22] as available in NWChem, was employed to investigate the possible multiconfigurational character of the wave functions of UDFT optimized $Ln(H_2O)_8^{3+}$ and $Ln(H_2O)_9^{3+}$ complexes containing unpaired electrons (Ln = Ce−Yb). In each case, the active space consisted of seven 4f orbitals with the respective amount of 4f electrons, starting at 1 for Ce and ending at 13 for Yb. Note that all calculations neglected spin−orbit (SO) effects within the 4f subshell. Prior spin−orbit configuration interaction and experimental studies have indicated that SO coupling constants are ∼2 kcal/mol in Ce(III) with an increase to ∼8 kcal/mol in Yb(III).[23,24] Given that the 4f electrons are not highly influenced by the ligand field these values are unlikely to change significantly for aqueous Ln(III). Errors within thermodynamic calculations should then cancel.

The hydration free energies in solution and thermodynamic properties of water addition were determined using the polarizable continuum model (PCM)[25] implemented in Gaussian 03. Single point PCM calculations on gas phase optimized structures were performed at the B3LYP level of theory with the UAKS cavity model,[26] using the default convergence criteria. We explicitly did not include counter-poise corrections to correct for basis set superposition error, as our prior work has shown that the magnitude of the correction for water addition reactions (using the successive reaction counterpoise scheme[27] or the standard counterpoise method of Boys and Bernardi[28]) to octa-aqua species is less than 1−2 kcal/mol in the gas phase, or ∼4−10%, and is consistent across the period.[14,16] Unrestricted single-point second-order Möller-Plesset (UMP2) perturbation theory calculations[29] were also performed at the optimized B3LYP geometries using the same basis with and without PCM to obtain UMP2 free energies of hydration and water addition energetics.

NWChem calculations were performed on the massively parallel Linux cluster in the Molecular Science Computing Facility in the William R. Wiley Environmental Molecular Sciences Laboratory (EMSL) at the Pacific Northwest National Laboratory (PNNL).

Results and Discussion

Geometric Information. It is well-established that the hydration coordination number (CN) of the trivalent lanthanides changes along the 4f period, with early Ln(III) having CN = 9, while equilibrium is established between CN = 9 and CN = 8 in the middle of the series, and late Ln(III) have CN = 8.[30−38] Study of both the

(12) Bylaska, E. J. et al. *NWChem, A Computational Chemistry Package for Parallel Computers*, Version 5.1; Pacific Northwest National Laboratory: Richland, WA, 2007.
(13) Frisch, M. J. et al. *Gaussian 03*, Revision C.02; Gaussian, Inc.: Wallingford, CT, 2004.
(14) Dinescu, A.; Clark, A. E. *J. Phys. Chem. A* **2008**, *12*, 11198.
(15) Clark, A. E. *J. Comp. Theory Chem.* **2008**, *4*, 708.
(16) Kvamme, B.; Wander, M. C. F.; Clark, A. E. *Int. J. Quantum Chem.* **2009**, *109*, 2474.
(17) (a) Becke, A. D. *J. Chem. Phys.* **1993**, *98*, 5648. (b) Lee, C.; Yang, W.; Parr, R. G. *Phys. Rev. B* **1988**, *37*, 785.
(18) Tao, J. M.; Perdew, J. P.; Staroverov, V. N.; Scuseria, G. E. *Phys. Rev. Lett.* **2003**, *91*, 146401.
(19) Dolg, M.; Stoll, H.; Preuss, H. *J. Chem. Phys.* **1989**, *90*, 1730.
(20) Cao, X.; Dolg, M. *J. Mol. Struct.* (*THEOCHEM*) **2002**, *581*, 139.
(21) Dunning, T. H., Jr. *J. Chem. Phys.* **1989**, *90*, 1007.
(22) Roos, B. O. In *Ab Initio Methods in Quantum Chemistry*; Lawley, K. P., Ed.; Wiley: New York, 1987; Vol. *2*, p 399.
(23) Sanoyama, E.; Kobayashi, J.; Yaushita, S. *J. Mol. Struct.* (*THEOCHEM*) **1998**, *451*, 189.
(24) Martin, W. C.; Alubas, R.; Hagen, C. Atomic Energy Levels−The Rare Earth Elements. In *Nat. Bur. Stand. Ref. Data Ser., Nat. Bur. Stand.* (*U.S.*) *Circ. No 60*; U.S. Government Printing Office: Washington, DC, 1978.
(25) Tomasi, J.; Mennucci, B.; Cammi, R. *Chem. Rev.* **2005**, *105*, 2999.
(26) Barone, V.; Cossi, M.; Tomasi, J. *J. Chem. Phys.* **1997**, *107*, 3210.
(27) Martin, J. M. L.; François, J. P.; Gijbels, R. *Theor. Chem. Acc.* **1989**, *76*, 195.
(28) Boys, S. F.; Bernardi, F. *Mol. Phys.* **1970**, *19*, 553.
(29) Moller, C.; Plesset, M. S. *Phys. Rev.* **1934**, *46*, 618.
(30) Allen, P. G.; Bucher, J. J.; Dhuh, D. K.; Edelstein, N. M.; Craig, I. *Inorg. Chem.* **2000**, *39*, 595.
(31) Cossy, C.; Barnes, A. C.; Enderby, J. E.; Merbach, A. E. *J. Chem. Phys.* **1989**, *90*, 3254.
(32) Cossy, C.; Helm, L.; Powell, D. H.; Merbach, A. E. *New J. Chem.* **1995**, *19*, 27.
(33) Habenschuss, A.; Spedding, F. H. *J. Chem. Phys.* **1979**, *70*, 2797.
(34) Habenschuss, A.; Spedding, F. H. *J. Chem. Phys.* **1979**, *70*, 3758.
(35) Habenschuss, A.; Spedding, F. H. *J. Chem. Phys.* **1980**, *73*, 442.
(36) Kanno, H.; Hiraishi, J. *J. Phys. Chem.* **1984**, *88*, 2787.
(37) Ohtaki, H.; Radnai, T. *Chem. Rev.* **1993**, *93*, 1157.

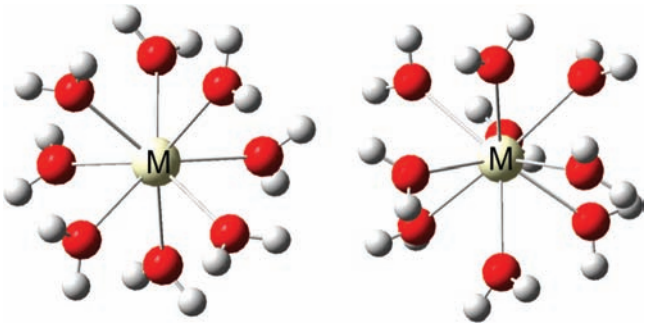

Figure 1. Square antiprismatic and tricapped trigonal biprismatic geometries adopted by $Ln(H_2O)_8^{3+}$ and $Ln(H_2O)_9^{3+}$, respectively.

nona- and octa-aqua species is thus relevant toward understanding the aqueous behavior of these ions. While we successfully optimized structures of $Ln(H_2O)_{8,9}^{3+}$ using UDFT, exceptions include Dy(III) and Ho(III), for which only the octa-aqua structure was obtained. With a single solvation shell of hydrating waters, using either the B3LYP or the TPSS functionals, a C_1 square antiprismatic (SAP) geometry is predicted for the 8-coordinate Ln(III). The CN = 8 hydrated structures of trivalent Ce, Pr, Nd, Sm, and Tb exhibited distortions wherein two $Ln-OH_2$ bond lengths were elongated and in the case of $Dy(H_2O)_8^{3+}$ three elongated $Ln-OH_2$ distances were observed. In the nona-aqua systems, a C_1 tricapped trigonal biprismatic (TTBP) geometry was predicted wherein the three average equatorial distances are longer than the average prismatic distances. Because of the contraction of the ionic radius, the extent of elongation of the equatorial bonds increases systematically along the lanthanide series, being the smallest for Ce(III) (>0.01 Å) and the largest for trivalent Tm, Yb, and Lu (~ 0.1 Å). Nevertheless, the average $Ln-OH_2$ bond distances decrease quadratically for both the 8- and 9-coordinate hydrates, as should be expected according to the lanthanide contraction and recent experimental studies of a homologous series.[8] The R^2 value for the quadratic fit to the sums of the calculated $Ln-OH_2$ bond lengths for the octa-aqua species is 0.9962, while for the nona-aqua species it is 0.9957 (see Supporting Information, Figure S1).

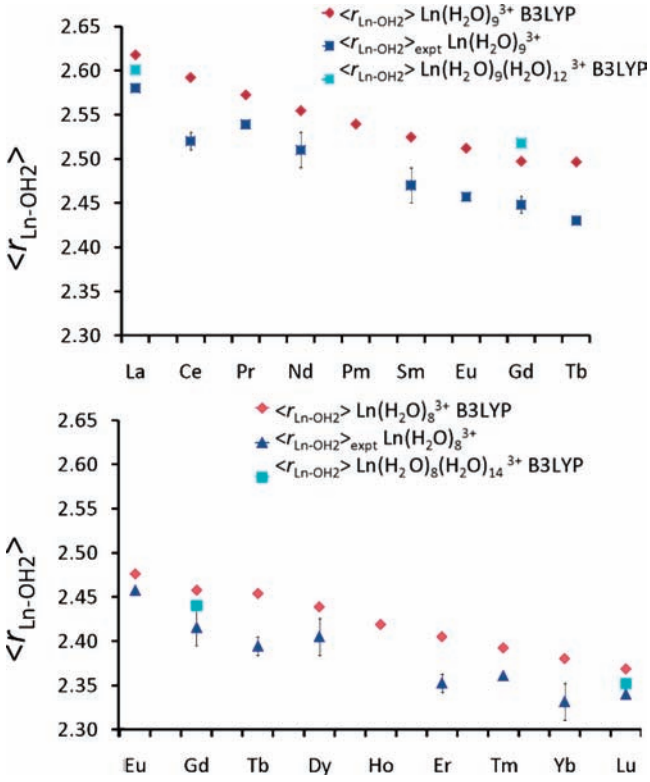

Figure 2. Average $Ln-OH_2$ bond lengths (in Å), as calculated by B3LYP/RSC28/aug-cc-pVDZ for Ln(III) = La−Lu in $Ln(H_2O)_{8,9}^{3+}$ and Ln(III) = La; Gd, and Lu in $Ln(H_2O)_{8,9}(H_2O)_{12,14}^{3+}$. Experimental values from refs 30−35, 38, 44, and 49.

A variety of solution- and solid-phase experimental data exist for hydrated Ln(III);[30−35,38−59] however, comparisons of calculated versus experimental structural data must be done carefully, as the reported $Ln-OH_2$ bond lengths are extremely sensitive to long-range interactions with counterions (see Supporting Information, Table S1). While octa-aqua species for the early trivalent lanthanides can be obtained in solutions with high ionic strength,[48,55,57,59] the counterions lie within 5 Å, which shortens the $Ln-OH_2$ bond lengths relative to the gas phase calculations. A variety of solution- and solid-state X-ray crystallographic and neutron diffraction data is presented in Supporting Information (Table S1). A plot of the calculated distances as well as selected experimental data for the entire 4f period is shown in Figure 2 and presented in Table 1. For the sake of clarity, only the average bond lengths calculated by the B3LYP combination of functionals for $Ln(H_2O)_{8,9}^{3+}$ and for $La(H_2O)_9(H_2O)_{14}^{3+}$, $Gd(H_2O)_9(H_2O)_{14}^{3+}$, $Gd(H_2O)_8(H_2O)_{14}^{3+}$, and $Lu(H_2O)_8(H_2O)_{14}^{3+}$ are shown; however, TPSS geometry optimizations produced similar results. Both Figure 2 and Table 1 clearly illustrate that the $Ln-OH_2$ bond lengths are systematically too long (by ~0.05 Å) when only a single solvation shell of water is present in the cluster. In some instances, the TPSS functional yields slightly "better" geometries than B3LYP for the primary solvation shell structures relative to experiment; however, the

(38) Yamaguchi, T.; Nomura, M.; Wakita, H.; Ohtaki, H. *J. Chem. Phys.* **1988**, *89*, 5153.
(39) Albertsson., J.; Elding, I. *Acta Crystallogr.* **1977**, *B33*, 1460.
(40) Annis, B. K.; Hahn, R. L.; Narten, A. H. *J. Chem. Phys.* **1985**, *82*, 2086.
(41) Barnes, J. C.; Nicoll, G. Y. R. *Inorg. Chim. Acta* **1985**, *110*, 47.
(42) Chatterjee, A.; Maslen, E. N.; Watson, K. J. *Acta Crystallogr.* **1988**, *B44*, 381.
(43) Faithfull, D. L.; Harrowfield, J. M.; Ogden, M. I.; Skelton, B. W.; Third, K.; White, A. H. *Aust. J. Chem.* **1992**, *45*, 583.
(44) Gerkin, R. E.; Reppart, W. J. *Acta Crystallogr.* **1984**, *C40*, 781.
(45) Harrowfield, J. M.; Kepert, D. L.; Patrick, J. M.; White, A, H. *Aust. J. Chem.* **1983**, *36*, 483.
(46) Helmholtz, L. *J. Am. Chem. Soc.* **1939**, *61*, 1544.
(47) Hubbard, C. R.; Quicksall, C. O.; Jacobson, R. A. *Acta Crystallogr.* **1974**, *B30*, 2613.
(48) Johansson, G.; Wakita, H. *Inorg. Chem.* **1985**, *24*, 3047.
(49) Johansson, G.; Wakita, H. *Inorg. Chem.* **1990**, *29*, 2460.
(50) Narten, A. H.; Hahn, R. L. *J. Phys. Chem.* **1983**, *87*, 3193.
(51) Näslund, J.; Lindqvist-Reis, P.; Persson, I.; Sandström, M. *Inorg. Chem.* **2000**, *39*, 4006.
(52) Ohki, Y.; Suzuki, Y.; Takeuchi, T.; Oughi, A. *Bull. Chem. Soc. Jpn.* **1988**, *61*, 393.
(53) Paiva Santos, C. O.; Castellano, E. E.; Machado, L. C.; Vicentini, G. *Inorg. Chim. Acta* **1985**, *110*, 83.
(54) Sikka, S. K. *Acta Crystallogr.* **1969**, *A25*, 621.
(55) Smith, L. S., Jr.; Wertz, D. L. *J. Am. Chem. Soc.* **1975**, *97*, 2365.
(56) Smith, L. S., Jr.; McCain, D. C.; Wertz, D. L. *J. Am. Chem. Soc.* **1976**, *98*, 5125.
(57) Smith, L. S., Jr.; Wertz, D. L. *J. Inorg. Nucl. Chem.* **1977**, *39*, 95.
(58) Steele, M. L.; Wertz, D. L. *J. Am. Chem. Soc.* **1976**, *98*, 4424.
(59) Steele, M. L.; Wertz, D. L. *Inorg. Chem.* **1977**, *16*, 1225.

Table 1. Structural Parameters of $Ln(H_2O)_8(H_2O)_x^{3+}$ (x = 0,14) and $Ln(H_2O)_9(H_2O)_x^{3+}$ (x = 0,12) within the First Solvation Shell Obtained at the B3LYP/RSC28/aug-cc-pVDZ Level of Theory Together with the Experimental Data Used on Figure 2[a]

Ln	$\langle r_{Ln-O}\rangle$	δ	$\langle r_{Ln-O}\rangle_{exp}$	ref.	Ln	$\langle r_{Ln-O}\rangle$	δ	$\langle r_{Ln-O}\rangle_{exp}$	ref.
$La(H_2O)_8^{3+}$	2.58	>0.01			$La(H_2O)_9^{3+}$	2.62	0.02	2.580(-)	34
					$La(H_2O)_9(H_2O)_{12}^{3+}$	2.60	0.03		
$Ce(H_2O)_8^{3+}$	2.55	0.02			$Ce(H_2O)_9^{3+}$	2.59	0.01	2.520(3)	30
$Pr(H_2O)_8^{3+}$	2.53	0.03			$Pr(H_2O)_9^{3+}$	2.57	0.03	2.539(-)	34
$Nd(H_2O)_8^{3+}$	2.51	0.02			$Nd(H_2O)_9^{3+}$	2.55	0.02	2.51(2)	38
$Pm(H_2O)_8^{3+}$	2.50	0.01			$Pm(H_2O)_9^{3+}$	2.54	0.03		
$Sm(H_2O)_8^{3+}$	2.48	0.02			$Sm(H_2O)_9^{3+}$	2.52	0.02	2.47(2)	32
$Eu(H_2O)_8^{3+}$	2.47	0.01	2.450(-)	35	$Eu(H_2O)_9^{3+}$	2.51	0.01	2.457(2)	44
$Gd(H_2O)_8^{3+}$	2.45	>0.01	2.41(2)	38	$Gd(H_2O)_9^{3+}$	2.50	0.05	2.446(2)	44
$Gd(H_2O)_8(H_2O)_{14}^{3+}$	2.43	0.11			$Gd(H_2O)_9(H_2O)_{12}^{3+}$	2.52	0.03		
$Tb(H_2O)_8^{3+}$	2.45	0.05	2.39(2)	38	$Tb(H_2O)_9^{3+}$	2.50	0.02	2.430(2)	44
$Dy(H_2O)_8^{3+}$	2.43	0.07	2.40(2)	31					
$Ho(H_2O)_8^{3+}$	2.41	0.01							
$Er(H_2O)_8^{3+}$	2.40	0.01	2.35(1)	49	$Er(H_2O)_9^{3+}$	2.45	0.06		
$Tm(H_2O)_8^{3+}$	2.39	0.01	2.358(-)	33	$Tm(H_2O)_9^{3+}$	2.44	0.10		
$Yb(H_2O)_8^{3+}$	2.38	0.01	2.33(2)	31	$Yb(H_2O)_9^{3+}$	2.43	0.09		
$Lu(H_2O)_8^{3+}$	2.37	>0.01	2.338(-)	33	$Lu(H_2O)_9^{3+}$	2.42	0.10		
$Lu(H_2O)_8(H_2O)_{14}^{3+}$	2.35	0.10							

[a] The range, δ, is defined as $r_{Ln-O\ longest} - r_{Ln-O\ shortest}$ in the CN = 8 species, while it is $\langle r_{Ln-O}\rangle_{equatorial} - \langle r_{Ln-O}\rangle_{prismatic}$ for the CN = 9 species.

frequencies for the Ln−OH_2 vibrational modes are nearly identical between functionals, with the symmetric stretch at ∼280 cm^{-1} and ∼330 cm^{-1} (non-scaled) for La-$(H_2O)_9^{3+}$ and $Lu(H_2O)_8^{3+}$, respectively. These values compare reasonably well with those reported experimentally at 316 cm^{-1} and 342 cm^{-1} for aqueous La(III) and Lu(III), respectively.[9]

More interesting geometric features are observed upon addition of a second solvation shell, which generally acts to contract the metal-water bond lengths in the primary solvation shell (by 0.02−0.07 Å), yielding values that are much closer to experiment than those obtained for the first shell by either B3LYP or TPSS. The nona-aqua Gd(III) species is an exception, whereby addition of a second solvation shell increases two equatorial and one prismatic bond length by 0.05−0.1 Å. This data point may be reflective of the equilibrium present between the CN = 9 and the CN = 8 species, with the octa-aqua species being energetically preferred according to our calculations (vide infra). Alternatively, the specific geometry of the second solvation shell may be far from a global minimum, perturbing the primary solvation sphere in an abnormal way. Prior molecular dynamics (MD) results support an equilibrium between 8- and 9-coordination for Gd(III): 8 by Yazyev et al.,[60] 8.4 by Villa et al.,[61] 8.62 by Clavaguera et al.,[62] 8.7 by Duvail et al.,[63,64] and 8.99 by Floris et al.[65] Our results thus imply that the lack of a second solvation shell is a dominant cause of the overestimation of the r_{Ln-OH2} bond length in Ln-$(H_2O)_{8,9}^{3+}$. The importance of the second solvation shell if further demonstrated by the calculated Ln−OH_2 vibrational frequencies within $La(H_2O)_9(H_2O)_{12}^{3+}$ and Lu-$(H_2O)_8(H_2O)_{14}^{3+}$, which lie between 248 and 314 cm^{-1} and 290−325 cm^{-1} (non-scaled) respectively. While a broader distribution of vibrational frequencies involving Ln−OH_2 is observed, several modes lie within 10 cm^{-1} of the experimental value of 316 cm^{-1} and 342 cm^{-1} for La(III) and Lu(III) hydrates, respectively.[9]

Geometry and f-Electron Configuration. In both the 8- and 9-coordinate species the highest degree of symmetry in the Ln−O bond lengths is observed for the f^0, f^7, and f^{14} elements [La(III), Gd(III), and Lu(III)], which implies that at the UDFT level, anisotropy of the f-electron configuration may alter the degree of symmetry of the gas phase structures. Some UDFT exchange-correlation functionals are known to prefer certain electron occupancies in highly symmetric systems, which may lead to an artificial symmetry breaking in the geometry.[66,67] However, in the clusters discussed here, the weak ligand field of the solvating waters already splits the f-orbital energies and the hydrogen bonding network of the first solvation shell yields an overall C_1 geometry. Recent computational studies by Groen at al. on $DyBr_3$ have also indicated that geometric parameters can be sensitive to the specific electronic state designated by the electron occupation of the f-orbitals.[68] To test this observation, the optimized C_1 $Ce(H_2O)_9^{3+}$ structure was symmetrized to C_3 so as to prevent mixing of the f-orbitals and examine the specific interactions between the f-subshell and the solvating waters. Within this symmetry, the water ligand field causes the Ce f-orbital manifold to have the f_{z^3} to be the lowest in energy, with the degenerate f_{xz^2} and f_{yz^2} higher in energy, followed by the $f_{x(x^2-3y^2)}$ and $f_{y(y^2-3x^2)}$ pair, and the f_{xyz} and $f_{z(x^2-3y^2)}$ pair to be the highest in energy. By swapping orbitals and forcing specific electron occupations, two different f-states were optimized using B3LYP. In the first ^2A state examined, the singly occupied orbital is the $f_{x(x^2-3y^2)}$, whose lobes lie along the bond axes of two of the capping waters (Figure 1). Here the optimized structure predicts metal-water bond lengths

(60) Yazyev, O. V.; Helm, L. **2007**, *127*, 084506.
(61) Villa, A.; Hess, B.; Saint-Martin, H. *J. Phys. Chem. B* **2009**, *113*, 7270.
(62) Clavaguera, C.; Calvo, F.; Dognon, J.-P. *J. Chem. Phys.* **2006**, *124*, 074505.
(63) Duvail, M.; Spezia, R.; Vitorge, P. *ChemPhysChem* **2008**, *9*, 693.
(64) Duvail, M.; D'Angelo, P.; Gaigeot, M. P.; Vitorge, P.; Spezia, R. *Radiochim. Acta* **2009**, *97*, 339.
(65) Floris, F. M.; Tani, A. *J. Chem. Phys.* **2001**, *115*, 4750.
(66) (a) Baerends, E. J.; Branchadelli, V.; Sodupe, M. *Chem. Phys. Lett.* **1997**, *265*, 481. (b) Schipper, P. R. T.; Gritsenko, O. V.; Baerends, E. J. *Theor. Chem. Acc.* **1998**, *99*, 329.
(67) Liu, W.; Dolg, M.; Li, M. *J. Chem. Phys.* **1998**, *108*, 2886.
(68) Groen, C. P.; Varga, Z.; Kolonits, M.; Peterson, K. A.; Hargittai, M. *Inorg. Chem.* **2009**, *48*, 4143.

of the aforementioned waters that are 0.04 Å longer than observed for the rest of the ligands, presumably because of a filled−filled repulsive interaction between the $f_{x(x^2-3y^2)}$ and the water lone-pair orbitals. The second ^2A state to be optimized had a single electron occupation of the f_{z^3} orbital, whose primary lobes of density run along the z-axis which is through the center of the pyramid of the biprismatic waters. The predicted geometry for this state has less repulsive interactions between the water lone-pairs and the filled f-orbital, and consequently lies 0.5 kcal/mol lower in energy than the $f_{x(x^2-3y^2)}$ configuration and has all r_{Ce-OH2} bond lengths within 0.01 Å of one another. Examination of the NPA atomic charges of the two different configurations does not reveal chemically meaningful differences between the two states; however, inspection across the entire period does indicate that f-electron configuration can impact the electrostatic interaction of the metal and water (vide infra).

Though errors associated with orbital degeneracy cannot be unequivocally ruled out, these results do indicate that hydration geometries (and necessarily reaction energetics) of $Ln(H_2O)_{8,9}^{3+}$ may be sensitive to specific f-orbital occupations. Interestingly, the geometric dependence upon f-electron configuration is overridden upon introduction of a second shell of hydrating waters, as the hydrogen-bonding interactions between solvation shells is stronger than the filled−filled interaction. The $La(H_2O)_9(H_2O)_{12}^{3+}$, $Gd(H_2O)_9(H_2O)_{12}^{3+}$, $Gd(H_2O)_8(H_2O)_{14}^{3+}$, and $Lu(H_2O)_8(H_2O)_{14}^{3+}$ clusters retain the essential SAP and TTBP structures within the primary solvation shell; however, the asymmetry of the Ln−OH_2 bond distances increases by an order of magnitude. Thus, the distribution of Ln−OH_2 bond lengths in the first coordination sphere of $Ln(H_2O)_{8,9}(H_2O)_{12,14}^{3+}$ is in the tenths of angstrom, while the distribution is in the hundredths of angstrom for $Ln(H_2O)_{8,9}^{3+}$. The enhanced *asymmetry* in the second solvation shell structures is nearly identical to that observed in our earlier work on Ce^{3+} (f^1)[16] and derives from strong hydrogen bonding and partial charge transfer between the waters of the primary and secondary solvation shells (vide infra). A similar observation was also made by Gutowski et al.[69] for UO_2^{2+}. These UDFT studies, of course, ignore dynamical effects in the second solvation shell; however, we are not concerned with the specific structure of extended solvation, merely its electronic and geometric impact upon the primary solvation shell, which is less likely to be dependent upon the effects of temperature and pressure.

Hydrogen Bonding. The hydrogen bonding networks present in the first and second solvation shells of the ion are reflective of the extent of water organization and are an integral component toward understanding the connection between geometry and the thermodynamics and kinetics of solvation. While the definition of a hydrogen bond is varied within the literature, we use the definition of Hammerich et al.,[70] where (i) the water oxygen is the nearest non-chemically bonded neighbor of the H-atom; (ii) the H-atom is the first or second nearest internuclear neighbor of the water oxygen. Additionally, we used a $r_{O\cdots H}$ cutoff distance of 3.0 Å, since beyond that point

(69) Gutowski, K. E.; Dixon, D. A. *J. Phys. Chem. A* **2006**, *110*, 8840.
(70) Hammerich, A. D.; Buch, V. *J. Chem. Phys.* **2008**, *128*, 111101.

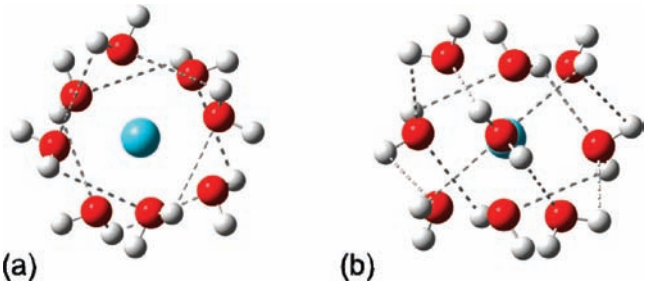

Figure 3. Representative hydrogen bonding networks in (a) $La(H_2O)_8^{3+}$ and (b)$La(H_2O)_9^{3+}$.

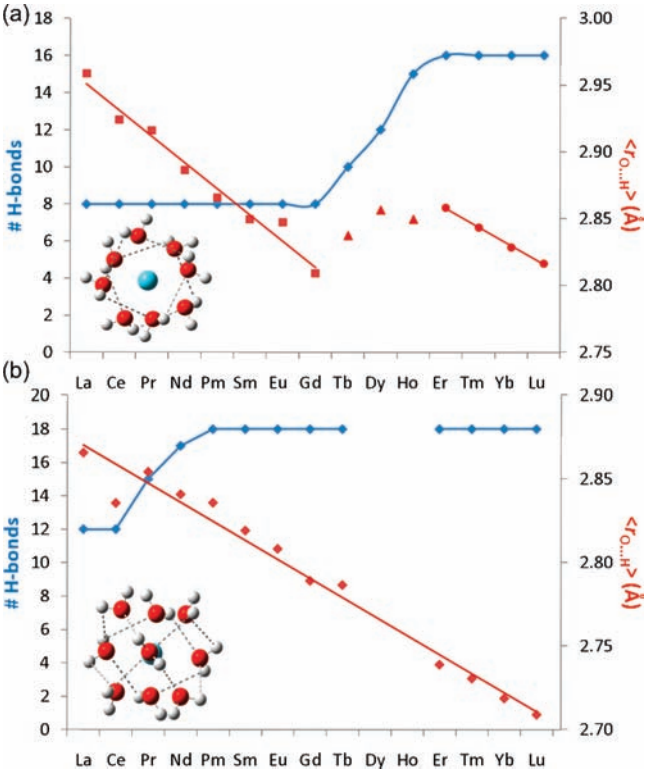

Figure 4. Number of hydrogen bonds (blue) and the average hydrogen bond lengths in Å (red) observed in (a) $Ln(H_2O)_8^{3+}$ and (b) $Ln(H_2O)_9^{3+}$.

orientation of the respective water molecules did not indicate the presence of the hydrogen bonding. Figure 3 illustrates the orientation of waters involved in hydrogen bonding within the first solvation shell of CN = 8 and CN = 9 species.

Examination of the hydrogen bonding networks present in $Ln(H_2O)_{8,9}^{3+}$, obtained from UDFT, across the 4f period yields several interesting trends. As seen in Figure 4a, the number of hydrogen bonds remains constant at ~8 for the octa-aqua complexes until Gd(III), after which the extent of H-bonding increases through Er(III), whereupon the maximal number of 16 is observed. In the nona-aqua species (Figure 4b), the lanthanide hydrates of La(III) and Ce(III) exhibit 12 H-bonds, which increases to the maximal number of 18 by the time Pr(III) is reached, remaining constant thereafter. Plotting the average hydrogen bond length across the period reveals a nearly linear decrease in $Ln(H_2O)_9^{3+}$ (R^2 = 0.9733), with a 0.08 Å decrease in H-bond length for every 0.1 Å decrease in ionic radius. However a bimodal distribution is observed in

$Ln(H_2O)_8^{3+}$. Between La(III) and Gd(III), where the H-bonding network is only half saturated, the O···H bond length decreases linearly ($R^2 = 0.9736$) at a rate of 0.14 Å for every 0.1 Å decrease in ionic radius (using Shannons ionic radii).[71] Starting at Er, the H-bonding network is fully saturated (16 H-bonds), and the bond length decreases linearly thereafter ($R^2 = 0.9972$) at a rate of 0.16 Å for every 0.1 Å decrease in ionic radius. Linear changes in H-bond length are not seen in the middle of the series (trivalent Tb, Dy, Ho), where the H-bonding network is intermediately saturated leading to more local minima on the PES, with a spread of H-bond lengths.

These data illustrate several important aspects of the primary solvation shells of trivalent Ln. Within the $Ln(H_2O)_8^{3+}$ the presence of only 1 H-bond for each water early in the series illustrates that the first solvation shell of La(III) through Gd(III) has much room to expand, rationalizing the preference of the CN = 9 species for those elements. Note too, that it is only at Er(III) that the number of H-bonds reaches its maximum value of 16. When the number of H-bonds per water molecule is < 2, the first solvation shell is likely more dynamic and capable of fluctuations relative to the completely saturated hydrogen-bonded systems. In the CN = 9 species, the extent of H-bonding becomes saturated early in the series, immediately after Ce(III). This indicates that La(III) and Ce(III), which have 12 and 16 hydrogen bonds respectively, may have some equilibrium with CN = 10 species. Indeed, several MD studies found high coordination numbers for La(III) in water: between 9 and 9.11,[72,73] between 9 and 10,[74,75] or even as high as between 10 and 12.[76,77] Thus, for ions with a single solvation shell, trends in H-bonding networks, their saturation, and O···H bond lengths may help to elucidate the availability of higher CN of an ion in solution. Upon addition of a second hydration shell, the interior waters no longer H-bond with themselves, instead reorienting to maximize H-bonding with the exterior waters. This makes sense as polarization and charge transfer between the two solvation shells is observed (vide infra).

Trends in Charge and Surface Charge Density. The trends observed in CN, hydrogen bonding, and even thermodynamic and kinetic features of solvation across the 4f period are primarily caused by the changes in the surface charge density (σ) of the ion, which may be defined as

$$\sigma = q/4\pi r^2 \qquad (1)$$

where q is the charge and r is the ionic radius. Assuming a formal charge on every Ln, and with the lanthanide contraction (using Shannon's ionic radii[71]), yields a nearly linear increase in σ across the period, with $R^2 = 0.998$ and 0.999 for the 8- and 9-coordinate species, and with slopes of 0.0044 and 0.0053, respectively. It is, however, possible for water to stabilize the high metal charge in solution through polarization and charge transfer, or for some coordinate covalent bonding to exist between the ion and solvating water molecules. As such, it is generally recognized that in solution, the charge of the ion will be smaller than 3+. Experimentally, this is known as the effective charge, q_{eff}, and has been derived from empirical observation. Empirical relationships between q, free energy of hydration, CN, r_{M-OH2}, and the crystallographic radius of the ion have long been known and perhaps originate with the Born equation.[78] Beginning in the early 1970s,[79,80] experimental observations initiated the derivation of numerous empirical equations that have aided in the evaluation of the hydration energies for the 4f and 5f elements and have been extended to electronic structure features like q_{eff}.[11,81−83] In particular, David has proposed an empirical hydration model for aquo ions that contain either a covalent or an ionic bond, and has been able to predict many interesting characteristics.[10,11] At its most simplistic, this model presumes a linear relationship between metal-water bond distance and the charge of the ion in solution. If experimental bond distances, d, are compared to those distances that result from a purely ionic model (with no charge transfer), d_{ionic}, then any deviations in these values, $\Delta d = d - d_{ionic}$, are assumed to be due to partial covalent bonding. Depending on the choice of experimental data for d, Δd may be observed to be largest early in the 4f period and to decrease to nearly zero by the middle of the series.[11] It stands to follow that if covalent bonding is the only mechanism that decreases the charge of an ion, the effective charge of lanthanoid ions must be the smallest early in the series and must increase across the period to a value near that of the formal charge. Based upon this model, the reported effective charges of the Ln(III) begin with values close to the formal charge, starting at 2.93 for La(III) and rising steadily to 2.99 at Lu(III).[11] Use of this data in eq 1 yields no significant difference in R^2 and slope of σ, relative to that observed with the formal charges.

It has been pointed out that quantum mechanical methods do not reproduce the proposed empirical trend of increasing charge across the 4f period.[10,11] While atomic charges calculated from orbital or spatial decomposition schemes are not physical observables, their trends often have chemical meaning, and we do observe that common population analysis schemes predict a decrease in Ln(III) charge across the 4f period that derives from partial charge transfer between solvating waters and the metal ion (Supporting Information, Table S3). As shown in Figure 5a, the UDFT/B3LYP calculated NPA charges start at ~2 for CN = 8 and decrease across the series. For the octa-aqua species, each water donates at least 0.13 e- to the metal ion, and the amount of charge stabilization provided by the water ligands increases across the period. The calculated charges of Dy in $Dy(H_2O)_8^{3+}$ and Er in $Er(H_2O)_9^{3+}$ are slightly aberrant relative to that of their neighbors, and the charge of Lu is consistently much more positive than that of its predecessors. The behavior of

(71) Shannon, R. D. *Acta Crystallogr.* **1976**, *A32*, 751.
(72) Duvail, M.; Spezia, R.; Cartailler, T.; Vitorge, P. *Chem. Phys. Lett.* **2007**, *448*, 41.
(73) Duvail, M.; Souaille, M.; Spezia, R.; Cartailler, T.; Vitorge, P. *J. Chem. Phys.* **2007**, *127*, 034503.
(74) Rode, B. M.; Schwenk, C. F.; Hofer, T. S.; Randolf, B. R. *Coord. Chem. Rev.* **2005**, *249*, 1993.
(75) Rode, B. M.; Hofer, T. S. *Pure Appl. Chem.* **2006**, *78*, 525.
(76) Kim, H.-S. *Chem. Phys. Lett.* **2000**, *330*, 570.
(77) Meier, W.; Bopp, P.; Probst, M. M.; Spohr, E.; Lin, J.-I. *J. Phys. Chem.* **1990**, *94*, 4672.
(78) Born, M. *Z. Phys.* **1920**, *1*, 45.
(79) Choppin, G. R. *Radiochim. Acta* **1983**, *32*, 43.
(80) Munz, R. *J. Inorg. Nucl. Chem.* **1972**, *34*, 661.
(81) Bratsch, S. G.; Lagowski, J. J. *J. Phys. Chem.* **1985**, *89*, 3317.
(82) Bratsch, S. G.; Lagowski, J. J. *J. Phys. Chem.* **1986**, *90*, 307.
(83) Mikheev, N. B.; Rumer, I. A. *Inorg. Chim. Acta* **1988**, *145*, 139.

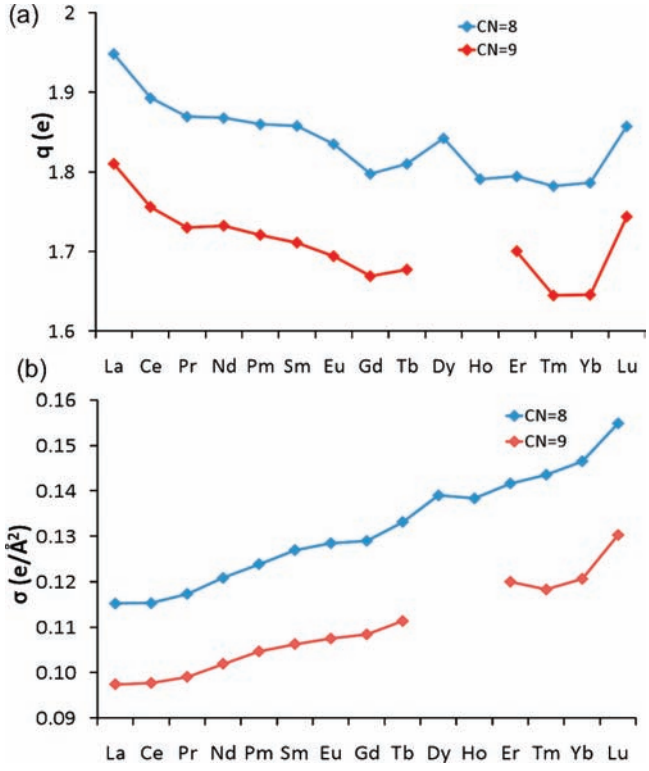

Figure 5. Natural charges (a) and surface charge density (b) on Ln for $Ln(H_2O)_x^{3+}$, where $x = 8$ or 9.

Lu(III) is understandable in light of its completely filled f-shell which will inhibit charge transfer from the oxygen lone-pairs of water, thereby increasing Lu's charge relative to Yb. Similar behavior is observed in the CN = 9 species, and owing to the extra H_2O ligand, the charge of the Ln(III) is smaller by an average of 0.13 e- relative to the CN = 8 case. Addition of a second solvation shell causes polarization and charge transfer from the exterior to interior waters, in turn further decreasing the metal charge by 0.05 to 0.16 e-. The question of coordinate covalent bonding between the metal and water ligand may be probed using natural bond order analysis (NBO).[84−86] Interestingly, according to B3LYP the only species that exhibit any Ln−OH_2 bonding orbitals are $La(H_2O)_9^{3+}$ and $Lu(H_2O)_{8,9}^{3+}$. In each case about 5% of the bonding orbital derives from the Ln d- orbitals and p-orbitals, whereas 95% comes from the O s- and p-orbitals. Thus, NBO predicts no covalent bonding interactions (sharing of electrons) for trivalent Ce−Yb hydrates and minimal bonding for La and Lu hydrates. The lack of bonding interactions for the majority of the series is further bolstered by our CASSCF calculations (vide infra). Here, extensive sharing of electrons between the Ln f-orbitals and the water ligands would lead to ligand-based orbitals within the active space. Based upon this data, the observed charge compensation of the metal from the water results from ionic interactions where the water oxygen atoms donate electrons to the metal in the absence of electron sharing. It is further evident that this electron donation

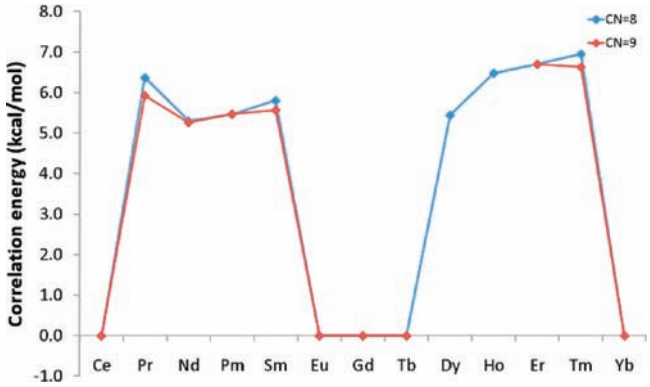

Figure 6. Correlation energy, calculated as $E_{ROHF} - E_{CASSCF}$ for $Ln(H_2O)_8^{3+}$ (blue) and $Ln(H_2O)_9^{3+}$ (red).

depends upon several factors, including hydration CN, the number of solvation shells, the metal ionic radius, and the f-orbital occupation. Thus, it is our contention that any empirical description of the metal water interactions must take into account charge transfer between the water ligand and the metal, which necessarily means that deviations in Ln−OH_2 bond lengths from an ideal number cannot immediately be attributed to "covalent interactions", as previously surmised.[10,11]

Since the decrease in ionic radius across the 4f period occurs more quickly than the decrease in calculated metal charge, the surface charge density calculated with the NPA data still increases across the period for both the CN = 8 and the CN = 9 species, with R^2 values near 1 (0.9781−0.959) and with slopes of ~0.002 (half of that observed when using the formal charge). Moreover, since the calculated charges increase when going from the nona- to octa-aqua species, at Gd, where the hydration number experimentally changes, a large increase in surface charge density is predicted as one jumps from the red line in Figure 5b to the blue.

Though the discrepancies between the current empirical model and our theoretical studies are clear, we note that the derivation of q_{eff} based upon Δd and ΔG_{hydr} is certainly not mathematically unique, and there are likely alternative forms and parameters that could yield both qualitatively correct free energies of solvation and agree with the proposed charge transfer stabilization of the ion in water, as calculated in this work.

CASSCF Wave Functions. Aside from La(III) and Lu(III) all members of the 4f period have unpaired f-electrons and can potentially display multiconfigurational character in their wave functions. The importance of the multiconfigurational wave function to bonding and electrostatic properties, in addition to the structure and thermodynamics of solvation, is unclear, and no systematic studies have been performed. Within this study, (n,7)CASSCF calculations were performed at the B3LYP optimized geometries of the aqueous clusters, where n is the number of unpaired 4f electrons. Both the wave function and the absolute energy were examined and compared to ROHF data to assess the role of multiconfigurational character upon the correlation energy in the system. Some multiconfigurational character is observed in systems that contain between 2 and 5 unpaired electrons (trivalent Pr, Nd, Pm, Sm, Dy, Ho, Er, Tm) (Supporting Information, Tables S4 and S5). In these cases, the correlation energy, calculated

(84) Reed, A. E.; Weinhold, F. *J. Chem. Phys.* **1983**, *78*, 4066.
(85) Reed, A. E.; Weinstock, R. B.; Weinhold, F. *J. Chem. Phys.* **1985**, *83*, 735.
(86) Reed, A. E.; Curtiss, L. A.; Weinhold, F. *Chem. Rev.* **1988**, *88*, 899.

as the energy difference between CASSCF and ROHF energies and plotted in Figure 6, is quite consistent across the period and is independent of the coordination number. Thus, this component of the energy should cancel when considering reaction energetics of the octa-aqua and nona-aqua species.

Free Energy of Hydration, ΔG_{hyd}, and Water Addition Reactions. The free energies of hydration for each trivalent cation were calculated at the UDFT/B3LYP level of theory using the following reaction:

$$Ln^{3+}{}_{(gas)} + (H_2O)_{8,9(aq)} \rightarrow Ln(H_2O)_{8,9(aq)}{}^{3+} \qquad (r1)$$

wherein the free energy in aqueous solution is defined by

$$\Delta G_{corr} = \Delta G_{gas}{}^{298.15} + \Delta\Delta G_{solv}{}^{tot} + SS_{corr} \qquad (2)$$

which has $\Delta G_{gas}{}^{298.15}$ as the free energy of reaction in the gas phase, $\Delta\Delta G_{solv}{}^{tot}$ as the solvation contribution to the free energy of reaction, and SScorr as the standard-state thermodynamic correction ($-4.3/n$ kcal/mol for each $(H_2O)_n$ water cluster according to B3LYP .[14,69,87] In the PCM, the solvation contribution to the free energy of a molecule can be expressed

$$\Delta G_{solv}{}^{tot} = \Delta G_{solv}{}^{elec} + \Delta G_{solv}{}^{nonelec} \qquad (3)$$

where $\Delta G_{solv}{}^{elec}$ is the electrostatic component of $\Delta G_{solv}{}^{tot}$, while $\Delta G_{solv}{}^{nonelec}$ is the sum of the non-electrostatic components of the $\Delta G_{solv}{}^{tot}$. For reaction 1, eq 3 can be written

$$\Delta\Delta G_{solv}{}^{tot} = \Delta\Delta G_{solv}{}^{elec} + \Delta\Delta G_{solv}{}^{nonelec} \qquad (4)$$

where,

$$\Delta\Delta G_{solv} = \Delta G_{solv}(Ln(H_2O)_{8,9}{}^{3+}) - \Delta G_{solv}(H_2O)_{8,9} \qquad (5)$$

All the contributions to the free energies of hydration for all the systems for UDFT and UMP2, where available, are provided in the Supporting Information (Tables S7 and S8). Our prior work has shown that the use of a molecular water cluster and a polarized continuum model with a UAKS cavity can yield very good estimates of ΔG_{hyd} for hard sphere cations.[14,88] Figure 7 presents the UB3LYP calculated ΔG_{hyd} values across the 4f period for the formation of the nona- and octa-aqua species, along with the experimental data of Rizkalla and Choppin[89] (Table 2 and Supporting Information, Table S7), while Table 2 presents both the B3LYP and UMP2 ΔG_{hyd} values. Interestingly, the UDFT data for both CN = 9 and CN = 8 species lies within the ~11 kcal/mol error bar of the experimental data (caused by inaccuracy of the

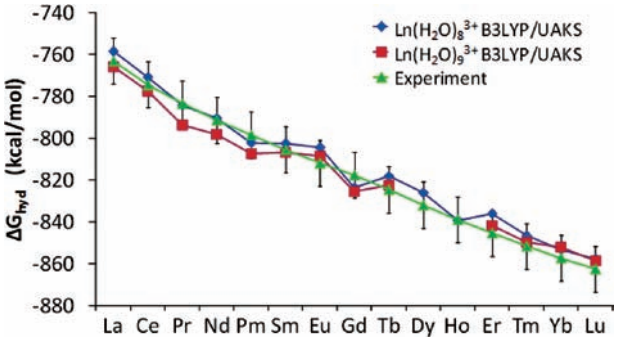

Figure 7. Calculated free energies of hydration, ΔG_{hydr}, (eqs 2−5) for reaction r1 based upon B3LYP/RSC28/aug-cc-pVDZ with the UAKS cavity in the PCM.

value of the free energy of aqueous H^+).[90] Early in the period, the UMP2 ΔG_{hyd} for the nona-aqua species are too negative by 15−20 kcal/mol, as are the ΔG_{hyd} values for the octa-aqua clusters late in the period. Addition of a second solvation shell also decreases the ΔG_{hyd} value by an additional 15−20 kcal/mol, making the values slightly lower than experiment. The exception to this observation is $Gd(H_2O)_9(H_2O)_{12}{}^{3+}$ where ΔG_{hyd} is 65 kcal/mol more negative than in $Gd(H_2O)_9{}^{3+}$. Interestingly, the geometrical parameters of $Gd(H_2O)_9(H_2O)_{12}{}^{3+}$ also had abnormally long Gd−OH_2 bond lengths, indicating that this particular structure may be far from the global minima for the second hydration shell which impacts the free energy of hydration.

Plotting the UDFT ΔG_{hyd} values (kcal/mol) for the first solvation shell structures as a function of the UDFT surface charge densities, σ (e/Å^2) results in two linear curves, wherein the free energy decreases significantly with increasing surface charge density. Specifically, the $Ln(H_2O)_9{}^{3+}$ species are highly sensitive to σ, with a slope of −3866 kcal e/mol Å^2 and the $Ln(H_2O)_8{}^{3+}$ species are much less sensitive, having a slope of only −1481 (Figure 8) . This is significant, as it may help understand differing reactivities between the early and late lanthanide hydrates and their complexation reactions.

The water addition reaction examined was

$$Ln(H_2O)_8{}^{3+}{}_{(aq)} + H_2O_{(aq)} \rightarrow Ln(H_2O)_9{}^{3+}{}_{(aq)} \qquad (r2)$$

where (aq) denotes use of a PCM to account for the bulk effect of the solvent dielectric. As shown in Table 3, the free energy of water addition becomes systematically less favorable across the 4f period; however, there are interesting deviations in the trend, and it does not appear to be linear. In general, the UDFT/B3LYP free energies are more negative for water addition to the early late lanthanides, accounting for the preference of $Ln(H_2O)_9{}^{3+}$, while later Ln^{3+} have positive ΔG_{rxn} indicating that the octa-aqua species is the dominant form. However, addition to $Pr(H_2O)_8{}^{3+}$ and $Er(H_2O)_8{}^{3+}$ seem abnormally favored (negative), while addition to $Gd(H_2O)_8{}^{3+}$ is quite unfavorable. To further probe the water addition thermochemistry, second order unrestricted Möller-Plesset perturbation theory (UMP2) was used in conjunction with the UAKS PCM model to determine the free energies of reaction 2. While convergence issues have limited our UMP2 data set for reaction 2 to 9 out of the 13

(87) Martin, L. R.; Hay, P. J.; Pratt, L. R. *J. Phys. Chem. A* **1998**, *102*, 3565.
(88) Wander, M. C. F.; Clark, A. E. *Inorg. Chem.* **2008**, *47*, 8233.
(89) Rizkalla, E. N.; Choppin, G. R. Hydration and hydrolysis of lanthanides. In *Handbook on the physics and chemistry of rare earths*; Gschneider, Jr., K. A., Eyring, L., Eds.; Elsevier Science Publishers: Amsterdam, 1991; Vol. *15*, p 393.
(90) Morss, L. R. *J. Phys. Chem.* **1971**, *75*, 392.

Table 2. Free Energies of Hydration (kcal/mol) in Aqueous Solution Using a PCM in Conjunction with UDFT/B3LYP/RSC28/aug-cc-pVDZ and UMP2/RSC28/aug-cc-pVDZ Levels of Theory with the UAKS Cavity

Ln	$\Delta G_{corr.}$ DFT	$\Delta G_{corr.}$ MP2	Ln	$\Delta G_{corr.}$ DFT	$\Delta G_{corr.}$ MP2	Exp
$La(H_2O)_8^{3+}$	−758.5	−768.2	$La(H_2O)_9^{3+}$	−765.9	−779.4	−763
			$La(H_2O)_9(H_2O)_{12}^{3+}$	−782.5		−763
$Ce(H_2O)_8^{3+}$	−770.9	−780.9	$Ce(H_2O)_9^{3+}$	−777.4	−790.9	−774
$Pr(H_2O)_8^{3+}$	−784.3	−789.4	$Pr(H_2O)_9^{3+}$	−793.8	−802.9	−783
$Nd(H_2O)_8^{3+}$	−790.5		$Nd(H_2O)_9^{3+}$	−798.2	−811.5	−791
$Pm(H_2O)_8^{3+}$	−802.2		$Pm(H_2O)_9^{3+}$	−807.4	−816.2	−799
$Sm(H_2O)_8^{3+}$	−802.5	−816.2	$Sm(H_2O)_9^{3+}$	−806.8	−822.8	−805
$Eu(H_2O)_8^{3+}$	−804.3	−822.0	$Eu(H_2O)_9^{3+}$	−808.6	−828.6	−812
$Gd(H_2O)_8^{3+}$	−823.6	−831.0	$Gd(H_2O)_9^{3+}$	−825.6	−836.9	−818
$Gd(H_2O)_8(H_2O)_{14}^{3+}$	−839.6		$Gd(H_2O)_9(H_2O)_{12}^{3+}$	−890.2		−818
$Tb(H_2O)_8^{3+}$	−818.2	−837.1	$Tb(H_2O)_9^{3+}$	−822.5	−844.9	−825
$Dy(H_2O)_8^{3+}$	−826.0					−832
$Ho(H_2O)_8^{3+}$	−839.2					−839
$Er(H_2O)_8^{3+}$	−836.0		$Er(H_2O)_9^{3+}$	−841.7		−845
$Tm(H_2O)_8^{3+}$	−846.6		$Tm(H_2O)_9^{3+}$	−849.8	−872.0	−852
$Yb(H_2O)_8^{3+}$	−853.0	−873.0	$Yb(H_2O)_9^{3+}$	−852.2	−875.4	−857
$Lu(H_2O)_8^{3+}$	−857.6	−876.7	$Lu(H_2O)_9^{3+}$	−858.5	−880.3	−863
$Lu(H_2O)_8(H_2O)_{14}^{3+}$	−877.0					−863

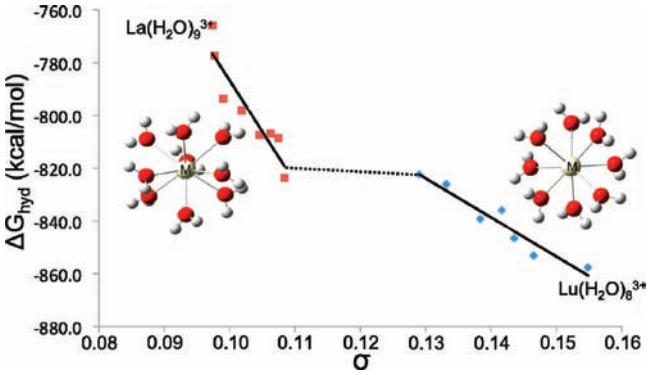

Figure 8. B3LYP/RSC28/aug-cc-pVDZ calculated free energies of hydration, ΔG_{hyd} (kcal/mol) versus the surface charge density, σ (e/Å^2), as calculated by eq 1 using the B3LYP NPA charges. $Ln(H_2O)_9^{3+}$ (Ln = La−Gd) are presented in red, while $Ln(H_2O)_8^{3+}$ (Ln = Tb−Lu) are presented in blue.

Table 3. Free Energies of Reaction 2 (kcal/mol) in Aqueous Solution (kcal/mol) Using a PCM in Conjunction with UDFT/B3LYP/RSC28/aug-cc-pVDZ and UMP2/RSC28/aug-cc-pVDZ Levels of Theory with the UAKS Cavity

$Ln(H_2O)_8^{3+}$ reactant	$\Delta G_{corr.}$ DFT	$\Delta G_{corr.}$ MP2
La	−3.9	−9.2
Ce	−2.8	−8.0
Pr	−5.9	−11.4
Nd	−4.3	
Pm	−1.8	
Sm	−0.9	−4.6
Eu	−0.8	−4.6
Gd	1.5	−3.8
Tb	−0.9	−5.8
Er	−2.3	
Tm	0.1	
Yb	4.2	−0.3
Lu	2.6	−1.5

lanthanide hydrates, the UMP2 ΔG_{rxn} are consistently about 4.5 kcal/mol lower in energy (more favored) than those calculated by B3LYP. Within the UMP2 data set, the same deviations from linearity are observed (Supporting Information, Table S9 and S10). It is possible that some of this behavior may be attributed to specific f-electron configurations influencing the favorability of the addition reaction, as implied by our structural data. To further test this hypothesis, we are currently optimizing specific f-electronic states and determining the water addition thermodynamics therein. This work is ongoing and will be the topic of future publications.

Conclusions

The current work has utilized UDFT, UMP2, and CASSCF calculations to probe the electronic and geometric structures of hydrated trivalent lanthanide ions, across the entire 4f period. As it pertains to the geometries adopted in solution, we observe that a second solvation shell is necessary for quantitative accuracy of bond lengths and vibrational frequencies and that the presence of these external waters is more important than the choice of functional, provided that the functionals behave similarly. In spite of this, interesting and useful data is obtained even when only a single solvation shell is present. For example, analysis of the hydrogen bonding networks correlates very well with CN preferences. Further, by fixing the f-orbital electron occupation, the UDFT Ln−OH_2 bond lengths can be modulated, presumably through alteration of the repulsive interactions of filled f-orbitals and water lone-pairs. Thus, the specific f-electronic state is important for geometric correlations in the primary solvation structures.

Hydrated species with 2−5 unpaired electrons were found to have correlation energies on the order of 5−7 kcal/mol, a value that is insensitive to the specific Ln metal as well as to coordination number, thus canceling when considering reaction energetics of the CN = 8 and CN = 9 species. The free energies of hydration calculated by B3LYP agree well with experimental values and when plotted against the surface charge density, reveal a bimodal distribution wherein the nona-aqua species are highly sensitive to σ while the octa-aqua species are much less dependent. The investigation of water addition to $Ln(H_2O)_8^{3+}$ reveals nearly identical trends in the reaction thermodynamics across the 4f period between UMP2 and UDFT. Both methods predict that formation of the nona-aqua species becomes less favored across the period; however, it is a non-linear function of the number of the surface charge density. Indeed, the aforementioned trends are widely believed to be governed by the surface charge density of the ion, which increases across the period because of the lanthanide contraction. A somewhat contentious issue within the literature pertains to the effective

charge of these ions and whether lanthanide-water covalent bonding influences bond distances and metal charge across the series. After a thorough electrostatic analysis we confirm the ionic nature of the $Ln-OH_2$ interaction and show that water significantly stabilizes the +3 charge of the ion through electron donation and that this effect is propagated across solvation shells.

Acknowledgment. A.E.C. recognizes support from the U.S. Department of Energy, Office of Nuclear Energy, Science and Technology, Junior Faculty Award Program award #DE-FG07-05ID14692/IDNE006. This research was performed using the Molecular Science Computing Facility (MSCF) in the William R. Wiley Environmental Molecular Sciences Laboratory, a national scientific user facility sponsored by the U.S. Department of Energy's Office of Biological and Environmental Research and located at the Pacific Northwest National Laboratory, operated for the Department of Energy by Battelle.

Supporting Information Available: Plots of the correlation of sum of $Ln-OH_2$ distances as a function of lanthanide, available experimental $Ln-OH_2$ distances, UDFT electronic energies, NPA and experimental charges, CASSCF data, correlation energies, UDFT and UMP2 determined and experimental free energies of hydration, UDFT and UMP2 determined water addition energetics and XYZ coordinates for the systems employed in current work. This material is available free of charge via the Internet at http://pubs.acs.org.